JOURNAL OF GEOPHYSICAL RESEARCH, VOL. 102, NO. D20, PAGES 23,819–23,828, OCTOBER 27, 1997

An investigation of measured temperature profiles and VHF mesosphere summer echoes at midlatitudes

Phillip B. Chilson,[1] Peter Czechowsky, Jürgen Klostermeyer, Rüdiger Rüster, and Gerhard Schmidt

Max-Planck-Institut für Aeronomie, Katlenburg-Lindau, Germany

Abstract. During the summers of 1992 and 1994, experiments were conducted in Germany (52°N) to investigate the region of the summer mesopause in connection with mesospheric summer echoes (MSE). MSE form in layers and are associated with dramatically enhanced radar scattering cross sections. Furthermore, since the summer mesopause is characterized by very low temperatures, it has been proposed that MSE layers are related to the presence of subvisible ice particles. Parallel measurements were made using the Sounding System (SOUSY) VHF radar and Rayleigh lidar. Radar observations showing MSE signatures are presented together with accompanying temperature profiles obtained from the lidar data. Generally, the ambient temperatures in the summer mesosphere at midlatitudes are above that required to create ice crystals. However, the presence of waves can reduce the temperature. Our observations show this to be the case. In particular, during one of the MSE events, two long-period inertia gravity waves were observed. These waves had estimated local periods of 6 and 8 hours with accompanying vertical wavelengths of 10 and 15 km, respectively. We find a good correlation between the locations of the calculated temperature minima and the observed MSE layers. Furthermore, the temperature minima were generally below the saturation temperature for water vapor, lending support to the supposition that the backscatter is connected with the presence of ice particles.

1. Introduction

Through the years the upper mesosphere/lower thermosphere has proven to be an intriguing region of the atmosphere. More than a decade ago, measurements made with the Poker Flat radar in Alaska showed the region to be even more intriguing through the discovery of layers near the polar mesopause associated with dramatically enhanced radar backscatter [*Ecklund and Balsley*, 1981]. Because these echoes only occur in the summer months, they have come to be referred to as polar mesosphere summer echoes (PMSE) [*Röttger et al.*, 1988]. Since the discovery of PMSE, there has been a growing interest in this phenomenon. Many observations of PMSE have been made using radar, lidar, and rockets, but the nature of the scattering processes and their generating mechanism remain an open question. The recent review articles by *Cho and Kelley* [1993] and *Hoppe et al.* [1994] provide summaries of the various observations and some of the recently proposed theories.

Among the various characteristic features of PMSE the ones that are relevant for this discussion are (1) an extreme enhancement in VHF radar scattering cross sections, (2) the correlation of PMSE with the summer polar mesopause region, (3) the very steep gradients in the electron density when PMSE are present, (4) the observed semidiurnal periodicity in the strength of PMSE signals and the occasional relationship of the signal strengths with long-period gravity waves, (5) the aspect sensitive nature of the scatter at VHF, and (6) the structure in the electron fluctuations below the viscous cutoff length [*Cho and Kelley*, 1993]. It is difficult to imagine a scattering mechanism that can account for all of these features. As discussed in *Cho and Kelley* [1993], turbulent fluctuations of the electron density do not provide a satisfactory explanation. Among other reasons the spectral widths of PMSE signals can be extremely narrow compared to typical coherent radar returns.

The occurrence of PMSE in the summer polar mesosphere is undoubtedly linked to the cold temperatures present in that region. In fact, the coldest naturally occurring temperatures of the Earth and its atmosphere are found near the summer mesopause. This fact has led to the proposal that PMSE are associated with clouds of subvisible ice particles, an idea that was already raised by *Ecklund and Balsley* [1981]. A temperature dependence could also explain the fluctuations in PMSE signal strengths with respect to tides and waves [*Rüster*, 1995b]. That is, ice particles could form and grow within the local temperature minima of the waves. However, pure Rayleigh scatter at VHF cannot account for the large observed echo strengths. In addition, the formation of ice particles alone is not sufficient to explain the experimental evidence linked with the electron density, namely, layers characteristic of sharp electron depletions (bite outs) and turbulent structures below the viscous cutoff range [*Ulwick et al.*, 1988; *Inhester et al.*, 1990; *Inhester and Ulwick*, 1992]. To account for these features, it has been proposed that PMSE result from charged ice particles or cluster ions [*Kelley et al.*, 1987; *Cho et al.*, 1992; *Cho and Kelley*, 1993; *Klostermeyer*, 1994; *Inhester et al.*, 1994; *Klostermeyer*, 1996].

Radar echoes similar to PMSE have also been detected in the summer mesopause at midlatitudes [*Czechowsky et al.*,

[1]Now at Swedish Institute of Space Physics, Kiruna, Sweden.

Paper number 97JD01572.
0148-0227/97/97JD-01572$09.00

Table 1. Radar and Lidar Parameters

	Radar	Lidar
Transmitter/Laser		
Wavelength	5.61 m	351 nm
Frequency	53.5 MHz	854.7 THz
Average power	24 kW	20 W
Pulse length	2 μs	20 ns
Height resolution	300 m	600 m
Sampling range	60–90 km	30–95 km
Receiving System		
Type of Receiver	Phased array, 196 Yagis	Cassegrain telescope, 12 m focal length
Diameter	72 m	0.8 m
Beam Width	5°	0.4 mrad
Beam Directions	5	1

1979; *Reid et al.*, 1989; *Thomas et al.*, 1992, 1996]. We will refer to these as mesosphere summer echoes (MSE). As a historical note, we mention that the observations made by *Czechowsky et al.* [1979] predate those of *Ecklund and Balsley* [1981]. That is, enhanced radar echoes associated with the summer mesopause region were actually first detected at midlatitudes. Although similar to PMSE, the frequency of occurrence of MSE is considerably smaller; they tend to be shorter in duration; and their backscatter enhancement is not as pronounced. This is most likely due to the fact that the ambient temperature of the summer mesopause increases with decreasing latitude, thus reducing the chances of ice particles forming. Indeed, the latitude range of 54°–57° has been given by *Thomas* [1991] as the lower limit of noctilucent clouds in the northern hemisphere.

In this paper we present complementary radar and lidar measurements collected in Germany (52°N) during the summers of 1992 and 1994 to investigate the structure of the summer mesopause region in conjunction with MSE. The measurements were made using the Sounding System (SOUSY) VHF radar and Rayleigh lidar. After describing the radar and lidar facilities we present examples of MSE detected by the radar during June of 1992 together with accompanying temperature profiles obtained from lidar data. Several typical features of both data sets are discussed. Additionally, we relate the height and temperature of the mesopause with the height and echo power of the MSE layers. Using radar and lidar data collected in July of 1991, we then present a case study of the effects of gravity waves on the temperature field and the formation of MSE. As we discuss below, MSE are detected by the SOUSY VHF radar during the day, whereas our lidar measurements are made during the night. However, using the lidar data and a simple gravity wave model, we have been able to simulate the thermal structure of the mesopause region during the time of an MSE event. These results are presented and discussed.

2. Observations and Data Processing

The SOUSY research group of the Max-Planck-Institut für Aeronomie has conducted or participated in several campaigns dedicated to the observation of PMSE/MSE events. These campaigns incorporated a host of experimental resources including atmospheric radars, lidars, and instrumented rockets. The existing observational data of PMSE and MSE correspond primarily to latitudes of 70°N and 50°N, respectively. Radar observations not only serve to identify the occurrence of MSE activity, but as will be shown, when MSE are present, the data also provide information relating to the dynamic structure of the ambient atmosphere at the time and location of the echoes. During clear-sky conditions, lidar data are useful in studying the temperature dependence of MSE.

The stationary SOUSY VHF radar is located in the Harz Mountains and has been in operation since the end of the 1970s. Through measurements of the signal strength of backscattered radiation along with its Doppler shift it is possible to use the radar to remotely deduce the scattering cross section and motion of atmospheric targets in the range of 2–30 and 60–90 km.

Remote sensing by radar techniques provides only a limited picture of the processes at work near the mesopause; therefore, to provide complementary data, a Rayleigh lidar has been constructed on site at the Max-Planck-Institut für Aeronomie. It operates at an ultraviolet wavelength and provides information on the density and hence temperature structure of the atmosphere between roughly 30 and 100 km. Here backscatter from the transmitted ultraviolet light pulses results primarily from Rayleigh scatter from air molecules with some occasional Mie scatter from aerosols or ice particles. The count rate of photons received at the surface is proportional to the atmospheric density. If hydrostatic equilibrium can be assumed, then the temperature may be calculated from the lidar data.

2.1. Radar

The SOUSY VHF radar is located at 51.65°N, 10.49°E and operates at a frequency of 53.5 MHz. The radar uses a phased array antenna that consists of 196 Yagi antennas and has a diameter of 72 m. The main beam of the array has a one-way half-power half width of 2.5° when directed vertically and can be steered over a continuous range of pointing angles. Only the parameters relevant to this experiment will be presented. A more thorough description of the system is given by *Schmidt et al.* [1979] and *Czechowsky et al.* [1984].

During the summer campaigns to investigate MSE the radar operated using the following parameters. The radar beam cycled through five orientations, one vertical and four off vertical. In this paper, however, we will focus on the data derived from the vertical beam. The sampling range for each beam was 60.0–95.7 km with a resolution of 300 m. A 16-bit complementary coded pulse was transmitted, and the received radar signal for each beam was stored as a 64-point complex time series [*Schmidt et al.*, 1979]. For each time series point, 52 coherent integrations were performed resulting in a sampling period of 0.17 s. The total dwell time for one beam was then 11 s. Data were stored to either magnetic tape or computer hard disk after every beam orientation. The total time required for one radar cycle was 59 s. A brief summary of the radar and some of the parameters used during the experiment has been given in Table 1.

Spectral analysis of the data was performed off-line. The signal power, radial velocity, and spectral widths were found from the first three spectral moments as calculated from the 64-pt time series data using a fast Fourier transform routine and analysis procedure similar to that described by *Rüster* [1994]. That is, each calculated moment corresponds to 11 s of radar data.

2.2. Lidar

The SOUSY UV lidar (51.64°N, 10.12°E) has been in operation since 1988. The transmitter channel consists of a XeF excimer laser (351 nm) with a maximum pulse energy of about

250 mJ, which can be stabilized on a constant level of 200 mJ for a continuous operation of about 6–8 hours. The pulse repetition frequency (PRF) of 100 Hz leads to a mean output power of 20 W. The beam divergence of the unstable resonator system was measured to be 0.4 mrad, illuminating a cylindrical volume with a diameter of only 40 m at an altitude of 100 km. The laser pulses are transmitted vertically into the atmosphere using dielectrically coated deflection mirrors with a reflectivity of about 99.5%. The photons scattered by air molecules and aerosols are collected by an 80-cm Cassegrain telescope with a total focal length of 12 m. The blur circle diameter of the system is 300 μm, which is a measure of the quality of the telescope resulting in a minimum field of view of 0.025 mrad. The effective beam width of the receiving system of 0.4 mrad (see Table 1), however, is given by the aperture and focal length and is matched to the divergence of the transmitter channel. The receiver channel is composed of an imaging lens system, an interference filter with a bandwidth of 3 nm, a sensitive photomultiplier, and a counter. The mechanical chopper protects the photomultiplier from overloading caused by strong Mie scattering within the altitude range below 30 km. The two optical axes of the telescope and the laser beam are separated by 0.8 m and are aligned by an adjustable mirror. The electronic components consist of a computer and a lidar controller synchronizing the pulse repetition, the chopper sequences, the multiplier counting rate, and the hardware adder. We again refer to the brief summary given in Table 1.

For the measurement campaigns to study MSE the lidar was operated with a height resolution of 600 m and a time resolution of 40 s. The power aperture product of the system enables count rates of 25 photons per laser pulse from an altitude of 35 km. After every 40 s (4000 shots) the profile of accumulated photon counts was written to a computer hard disk. The upper range of the observations depends on the sky conditions and the amount of integration time. Typically, the temperature profiles to be discussed in this work extend up to 88–90 km.

When processing the lidar data to obtain the density and temperature profiles, a method similar to that of *Chanin and Hauchecorne* [1980] was used. Note that a detailed description of the procedure is given by *Shibata et al.* [1986]. For each count rate profile the background noise was subtracted, and then the profiles were averaged. From the count rate data the atmospheric density was calculated. Next, the temperatures are calculated from the density profiles. Here the upper limit of the temperature profile was determined as the lowest altitude for which the standard deviation of the temperature exceeded a predetermined limit. Further information pertaining to the SOUSY UV lidar is given by *Czechowsky et al.* [1991], which describes a comparison between polar mesosphere winter echoes and lidar-derived temperature that was performed in Andenes, Norway, during 1990.

3. Analysis and Results

Given the limited amount of moisture at altitudes where PMSE/MSE form, very low temperatures are required to promote the creation and growth of ice particles. An equation relating the saturation pressure p_{sat} of water vapor over a plane ice surface to the ambient temperature T has been given by *Gadsen* [1981] as

$$p_{sat} = \exp\left(28.548 - \frac{6077.4\ \mathrm{K}}{T}\right)\ \mathrm{Pa} \qquad (1)$$

This expression is valid in the temperature range from 100 to 220 K. For a given value of the water vapor mixing radio w and the atmospheric pressure p, (1) can be written in terms of the saturation temperature

$$T_{sat} = \frac{6077.4\ \mathrm{K}}{28.548 - \ln w - \ln p} \qquad (2)$$

Using (2), we can now estimate the temperatures required for ice particles to form in conjunction with PMSE/MSE occurrences. In the calculation we use a pressure of 0.61 Pa, taken from the 1986 COSPAR International Reference Atmosphere (CIRA-86) for July at a height of 85 km and a latitude of 70°N [*Fleming et al.*, 1990]. Assuming a water mixing ratio of 1 ppmv, we find a saturation temperature of 142 K. Performing the calculation again, but this time for a latitude of 50°N (0.51 Pa), we arrive at a saturation temperature of 141 K, similar to that for the polar latitudes. For comparison we have calculated the saturation temperature using the empirical data of *Lübken and von Zahn* [1991] measured at 69°N during July. At a height of 85 km, T_{sat} = 141 K for a water mixing ratio of 1 ppmv.

In a recent paper by *Inhester et al.* [1994], VHF radar observations of PMSE together with temperature profiles derived from falling sphere data have been compared. These data were obtained during the Middle Atmospheric Cooperation (MAC)/Summer in Northern Europe (SINE) campaign near Andenes, Norway. On the basis of 22 individual temperature profiles taken while the radar was in operation they observed that (1) more than 80% of the observed PMSE events occurred at temperatures below 140 K, (2) at the bottom side of the PMSE layer the temperatures deviated by no more than 5 K from 140 K in more than two thirds of the cases, (3) the frequency of occurrence or the echo strengths did not show a significant correlation with the local temperature, and (4) more echoes appear below the temperature minimum than above [*Inhester et al.*, 1994]. In regards to the last point, *Inhester et al.* [1994] state that the zero-order estimate of the location of the echo maximum with the temperature minimum is probably not well supported. In the next section we present complementary data showing examples of MSE together with the corresponding thermal structure of the mesopause region.

3.1. Examples of Radar and Lidar Data

The likelihood of observing MSE with the SOUSY VHF radar is limited by its location, namely, the latitude. According to *Hall* [1995], the radar lies at the southern tip of the boundary delineating a region in the northern hemisphere in which PMSE/MSE activity is to be expected. Furthermore, at 52°N latitude the MSE season lasts only for roughly 8 weeks. Compounded with that, reliable lidar measurements can only be made during clear-sky, and preferably new moon, conditions. Therefore we have only a limited number of cases in our data which facilitate an analysis of the mesopause temperatures in conjunction with radar observations of an MSE event.

A partial explanation of the differences between PMSE and MSE can be found by examining the thermal structure of the mesopause at different latitudes. In Figure 1 we show temperature profiles for July taken from CIRA-86 [*Fleming et al.*, 1990] together with empirical data from *Lübken and von Zahn* [1991] (69°N). The model temperature minimum for polar regions lies approximately 15 K below that for midlatitudes. Note that the observed temperature data for 69°N are 10 K below the 140 K reference line. An additional difference is that the polar mesopause is "narrower" than at midlatitudes. That

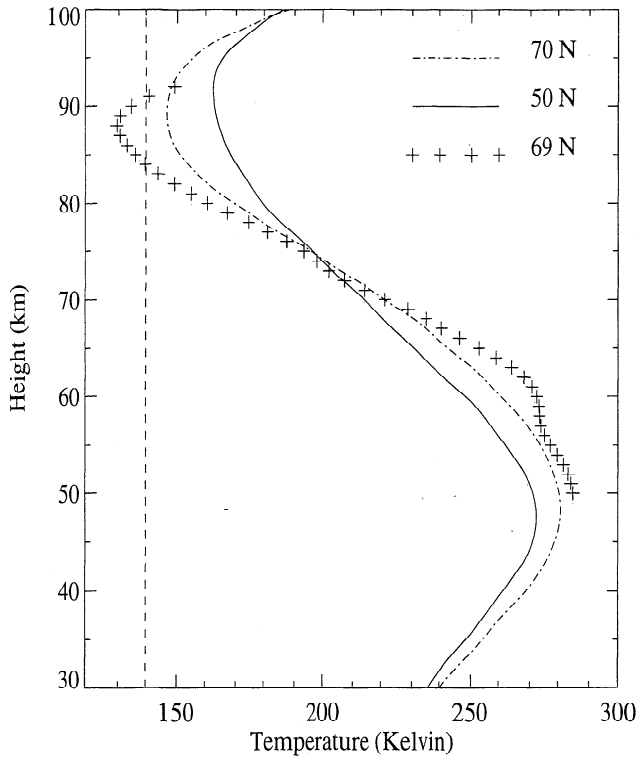

Figure 1. Height profiles of temperature for July taken from 1986 COSPAR International Reference Atmosphere (CIRA-86) (50°N and 70°N) [*Fleming et al.*, 1990] and observations (69°N) [*Lübken and von Zahn*, 1991]. The vertical dotted curve indicates a 140 K reference temperature.

is, the absolute value of the temperature gradients on either side of the polar temperature minimum are larger than those for the midlatitude minimum. Consequently, it is much more likely for ice particles to form at polar latitudes than at midlatitudes.

Examples of radar and lidar observations taken during the summer of 1992 are given in Figures 2 and 3. These examples do not represent the only data obtained in 1992 for which complementary radar and lidar observations were made. However, the data set is rather unique in that sky conditions permitted lidar observations to be made on 5 out of 6 consecutive nights. Furthermore, the temperature profiles could be derived for up to 90 km in all five cases.

Figures 2a–2f correspond to observations made on 6 consecutive days in June using the vertical radar beam. Each panel shows the backscattered snr for the respective days. For the presentation in Figure 2 the signal-to-noise ratio (snr) values have been averaged using six consecutive vertical beam observations, giving a time resolution of around 6 min. Here we notice two examples of MSE layers occurring on June 25 (Figure 2a) and June 28 (Figure 2d). The intermittent black vertical segments located primarily between 80 and 90 km indicate meteor echoes. Note that during the course of the observations, radar complications resulted in several data gaps. The most noticeable of these occurred on June 28 from 1459 to 1550 LT and on June 30 from 0522 to 0809 and 0934 to 2400.

Already, in this limited set of observations we can notice some features of MSE typically observed with the SOUSY VHF radar. The echoes occur preferentially between roughly 0600 and 1800 LT in relatively thin layers at heights between 75 and 85 km. In contrast to the observations of PMSE made at high latitudes, we rarely see double-layer structures with a small vertical separation [*Reid*, 1990]. All of the examples shown in Figure 2 demonstrate a downward propagation. Although not seen in all cases, the downward propagation is a frequently observed feature of MSE seen with the radar. Furthermore, since the SOUSY VHF radar lies at the lower boundary of the latitude range in which MSE observations are expected, we cannot detect such echoes daily. In Figure 2 the two most prominent MSE events are separated by 3 days; however, on the basis of other observations of MSE with the SOUSY VHF radar, separations of 5–6 days appear to be more common. A 5–6 day periodicity could result from waves [e.g., *Manson et al.*, 1981a, b] or a cycling of proton hydrates [*Sugiyama et al.*, 1996].

We examine the lidar data to see if any correlation can be observed between the occurrence of MSE and the temperature. As already mentioned, MSE are typically observed by the radar between 0600 and 1800 LT. However, usable lidar measurements can only be obtained during dark-sky conditions, which during the summer, lie between approximately 2300 and 0300 LT. Therefore a test of the correlation between the radar and lidar observations cannot be performed. However, a comparison of the temperature profiles derived from nighttime lidar observations and daytime radar observations of MSE does provide useful information [*Thomas et al.*, 1996].

The five temperature profiles in Figure 3 are shown together with the CIRA-86 temperature data for June at a latitude of 50°N. The lidar-derived temperatures match those from CIRA-86 fairly well between the heights of 30 and 70 km. Above 70 km, however, we notice considerable deviations between the two. First, the values of the minima in the derived temperature profiles are lower than those of CIRA-86. Second, these minima are lower in altitude and more sharply peaked than for CIRA-86. Last, considerable structure can be seen in the measured temperature data.

What information can we extract from the data presented in Figures 2 and 3? The most obvious feature in the profiles of Figure 3 is that the mesopause temperature lies below 140 K on 3 of the 5 nights and below 142 K on 4 of the 5 nights. Another obvious feature of the temperature profiles is the oscillatory structure indicating the presence of atmospheric waves. In fact, the wave patterns on the temperature profiles sometimes result in two distinct temperature minima, making it difficult to locate the exact height of the mesopause. The values of the temperature minima for each night and the heights at which they occurred are given in Table 2.

The data shown in Figures 2 and 3 can be compared with results from *Thomas et al.* [1996], who recently demonstrated the relation between the thermal structure of the midlatitude mesosphere and radar echoes measured in all seasons. In their study they used a colocated VHF radar and a Rayleigh lidar at Aberystwyth (52°N, 4°W). *Thompson et al.* [1996, pp. 12,870–12,871] stated "These comparisons of temperature profiles for individual nights with radar echoes during the preceding and succeeding daytime periods demonstrate the clear association between the echoes and low mesopause temperatures at a given site." Unlike the lidar data of *Thomas et al.* [1996] our data showed no signs of Mie scatter from ice particles.

In our data we also notice an association between the occurrence of MSE and the thermal structure near the mesopause. The strongest and most prominent examples of MSE shown in Figure 2 occurred on June 25 and 28. The echo layer

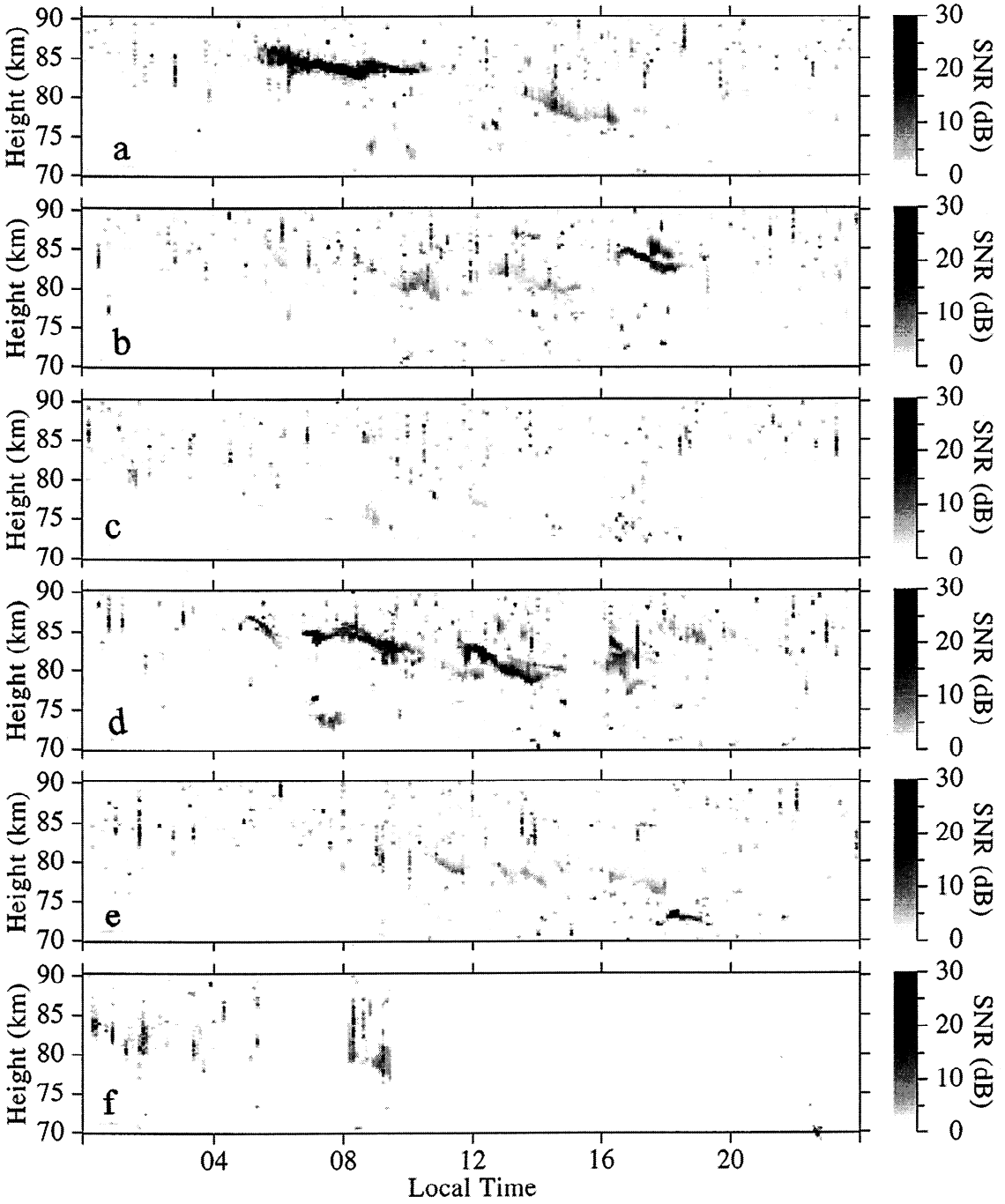

Figure 2. Time-height plots of the vertical beam snr from June 25–30, 1992. The dates associated with each panel increase from Figure 2a to Figure 2f. That is, Figure 2a and Figure 2f show the data for June 25 and June 30, respectively.

of June 25 (Figure 2a) begins around 0530 LT at an altitude of 85 km and persists for approximately 6 hours. The peak snr within the layer is 43.5 dB. Note that the snr scale in the figure only extends to 30 dB to emphasize the weaker echoes. The temperature profiles for the nights of June 24/25 and 25/26 are both near or below the saturation temperature of 141 K for an assumed pressure and water mixing ratio of 0.52 Pa and 1 ppmv, respectively. Furthermore, both temperature minima were located at a height of 84.6 km. The second most prominent MSE occurred on June 28 (Figure 2d). On this day the layer is not continuous and exhibits a noticeable descent. As we will show in the next section, these two features are indicative of gravity waves. Here the layer begins around 0700 LT at a height of 85 km, and although not continuous, the layer persists over a period of roughly 12 hours. The peak snr value is 36.3 dB. Unfortunately, we do not have any temperature information for the night following the MSE layer, but on the preceeding night the temperature profile shows two minima of 144.5 and 132.6 K at altitudes of 84.6 and 87.6 km, respectively. Although the radar and lidar measurements were not simultaneous, we note that the MSE layers of June 25 and 28 correspond to profiles having the two lowest derived temperature

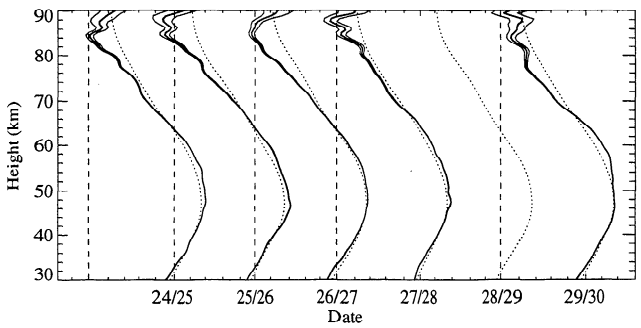

Figure 3. Temperature profiles (heavy solid curves) obtained from 5 nights of lidar observations spanning June 24–30, 1992. The standard deviations are shown as light solid curves derived from lidar observations, and the vertical dashed curves indicate a 140 K reference temperature. The dotted curves show temperature profiles taken from CIRA-86. Each temperature profile has been offset by 100 K, and the tick marks are separated by 20 K. See Table 2.

minima, with the lower of the two being associated with the layer of June 25. The low mesopause temperatures could be considered a necessary but not sufficient condition for MSE. As evidence, we see that although the day of June 26 is preceeded and followed by low mesopause temperatures, only a brief MSE signature can be seen.

Although these measurements show the connection between the thermal structure of the upper mesosphere/lower thermosphere and MSE, we must be careful in our interpretation. Irrespective of the good agreement found between the height and temperature of the mesopause and the occurrence of the MSE layers, the fact remains that the radar and lidar observations are separated by as much as 12 hours. In the next section we present a method to circumvent this problem.

3.2. A Case Study Comparison of Radar and Lidar Data

A particularly fortuitous case of radar/lidar observations during an MSE event occurred between July 12 and 14, 1994. On July 13 an MSE was detected that lasted roughly 8 hours and extended over a height range of 10 km. Additionally, the nights before and after the event provided favorable conditions for lidar observations. During the first nighttime quality of the lidar data permitted temperature profiles having acceptable uncertainty levels to be generated from 45 min data segments. Consequently, a series of five temperature profiles could be constructed. On the second night, however, it was only possible to produce a single temperature profile. These data have been used for a case study analysis of an MSE in connection with the interpolated ambient temperature field.

The analysis that we present in this study relies on the validity of a few central concepts. First, the position of an MSE layer in time and height is close to locations of temperature minima in the atmosphere. We have already presented evidence of that in section 3.1. The works of *Inhester et al.* [1994], *Thomas et al.* [1996], and *Nussbaumer et al.* [1996] provide further support. Next, oscillations of the ambient temperature in time and height result from the presence of atmospheric waves [*Jensen and Thomas*, 1994]. The effects of a gravity wave on atmospheric temperature [*Chanin and Hauchecorne*, 1981; *Meriwether et al.*, 1994] and density [*Namboothiri et al.*, 1996] have already been reported. For the latter case the gravity wave, which had an intrinsic period of 9.1 hours and vertical and horizontal wavelengths of 16 and 1900 km, respectively, was detected by radar and lidar. Finally, these two themes are united in the papers by *Rüster* [1995a] and *Cho and Morley* [1995]. These authors obtained temperature variations from the observed velocity field and related them to the signal power in PMSE layers.

A portion of the radar data obtained on July 13 has been presented in Figure 4. Here we show the first three spectral moments for the vertical beam plotted as a function of height and time. The moments are represented as the power, Doppler velocity, and the spectral width in Figures 4a, 4b, and 4c, respectively. The data shown in Figure 4 have been processed using six spectral averages, yielding a time resolution of approximately 6 min. Comparing the MSE of July 13 with the ones shown in Figure 2, we note that the echo intensity is rather weak. The peak snr value is 28 dB. However, two features of the MSE event make it particularly interesting in connection with the lidar observations. One is the occurrence of two layers at 0800 LT, and the other is the rapid downward motion of the layer with time.

Assuming that the occurrence of the MSE layers is linked with local temperature minima, we can extract wave parameters from the radar data to investigate the structure of the ambient temperature field [*Lübken et al.*, 1995; *Klostermeyer*, 1996; *Nussbaumer et al.*, 1996]. First, we note that from ~0700 to 1000 LT, two layers are present with a separation of about 10 km. The lower layer occurs at an altitude below that typically associated with PMSE/MSE activity. We address this point below. The upper layer descends at a rate of roughly 2.3 km h^{-1} (0.64 m s^{-1}). Using 10 km as the vertical wavelength and 2.3 km h^{-1} as the phase propagation, we calculate the local wave period to be 4 hours. A further example of atmospheric waves in the radar data are the 1 hour oscillations in the values of the Doppler velocities and their spectral widths.

We have adopted an approach that permits us to extrapolate the temperature measurements from the night to the time the MSE layer occurred in the radar data. This involved first assuming a simple gravity wave model for the atmosphere during the time of the observations. The parameters for the model were obtained from a harmonic analysis of the five lidar-derived temperature profiles for the night of July 12/13. The gravity wave model was then used to extrapolate the temper-

Table 2. Summary of the Lidar Measurements for June 1992

Date	Time, LT	Derived Profile Minima: Height, km	Derived Profile Minima: Temperature, K
24/25	2334–0159	84.6	141.3* ± 3.8
		87.6	150.9 ± 8.8
25/26	2332–0104	84.6	129.3* ± 4.6
		88.2	127.6* ± 10.6
26/27	2337–0256	85.2	135.4* ± 4.0
		...	...
27/28	2334–0126	84.6	144.5 ± 4.6
		87.6	132.6* ± 7.7
28/29	...	...	...
		...	...
29/30	2330–0130	84.0	151.4 ± 4.7
		89.4	143.2 ± 14.8

*Temperature values believed to lie below the saturation temperature for water vapor.

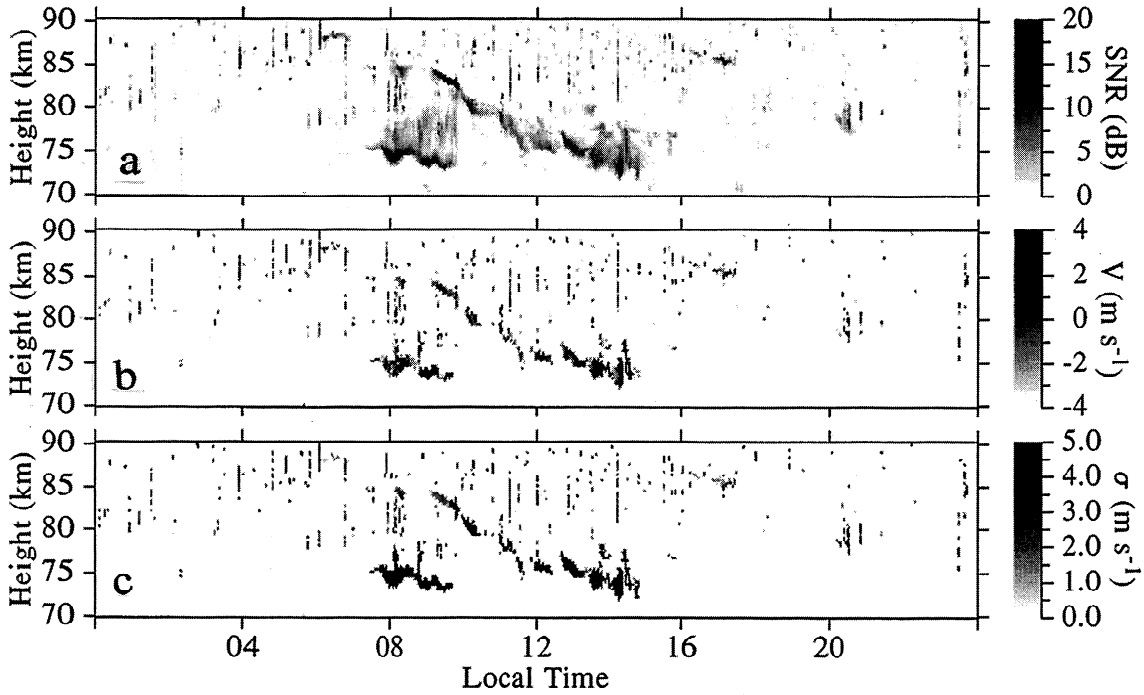

Figure 4. Time-height plots of the vertical beam data for July 13, 1994: (a) the snr, (b) the radial velocity, and (c) the spectral width.

ature measurements to those of the following night, July 13/14, for which a single temperature profile is available.

The temperature data for the period of July 12–14 are shown in Figure 5 for the height range of 60–90 km. As in Figure 3, the profiles have been offset by 100 K, and the vertical dashed curves mark the 140 K point. The effects of gravity waves can be clearly seen in the profiles. A summary of the times and locations of the temperature minima is given in Table 3.

We present an outline of the procedure used to model the temperature field during the time of the MSE layer shown in Figure 4. First, the five temperature profiles for the night of July 12/13 were time-averaged. The result was then fitted to a parabola in the height range of 60–80 km using the equation

$$T_B(z) = A(z - z_{\min})^2 + T_{\min} \tag{3}$$

where T_B is the background temperature, A is a constant, and $z_{\min}$ and $T_{\min}$ are the minimum height and temperature values, respectively. The background temperature profile was then subtracted from the calculated temperature values giving five profiles of the perturbed temperature. Finally, each profile of the perturbed temperature T_P was fitted using the equation

$$T_P(z) = \sum_{n=1}^{N} T_n e^{(z/2H)} \cos\,(m_n z - \omega_n t + \phi_n) \tag{4}$$

where H is the atmospheric scale height. The amplitude, vertical wavenumber, local frequency, and phase of the wave n are

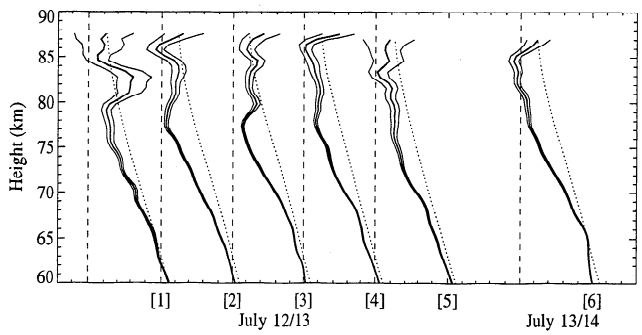

Figure 5. Temperature profiles for two nights in July of 1994 presented using the same format as in Figure 3. The first five profiles are for the night of July 12–13, and the last profile is for the night of July 13–14. See Table 3.

Table 3. Summary of the Lidar Measurements for July 1994

Date	Time, LT	Derived Profile Minima: Height, km	Derived Profile Minima: Temperature, K
12/13	2318–0319	78.0	162.6 ± 2.0
		85.8	135.7* ± 7.6
12/13 [1]	2321–0004	79.2	163.4 ± 7.2
		85.2	151.1 ± 18.3
12/13 [2]	0004–0047	77.4	146.6 ± 2.5
		85.8	131.7* ± 11.0
12/13 [3]	0048–0130	77.4	154.3 ± 2.0
		85.8	160.4 ± 11.4
12/13 [4]	0146–0229	78.0	156.3 ± 2.4
		85.8	142.3 ± 8.4
12/13 [5]	0253–0335	81.0	159.0 ± 7.5
		83.4	142.4 ± 12.4
13/14	0036–0142	82.8	134.7* ± 4.6
		84.6	129.7* ± 6.8

The numbers in the brackets are used to label the profiles and are the same as those given in Figures 5 and 6.

*Temperature values believed to lie below the saturation temperature for water vapor.

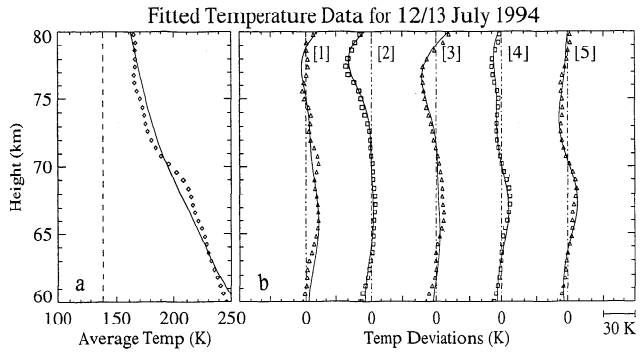

Figure 6. (a) Profile of the time-averaged temperature data (diamonds) and the fit (solid curve) from (3). (b) Profiles of the gravity wave perturbations to the temperature field (alternating triangles and squares) and the fits (solid curves) from (4). The numbers in the brackets are used to label the profiles and are the same as given in Figure 5 and Table 3.

given by T_n, m_n, ω_n, and ϕ_n, respectively. We chose to use two waves ($N = 2$) in (4) for the simple reason that one wave did not adequately model the data, and we did not have sufficient temperature information to justify a fit using three waves.

The fitting procedure has been implemented using the temperature data for July 12/13, and the results are shown graphically in Figure 6 and numerically in Table 4. Because of such effects as breaking gravity waves and reduced snr in the photon counts, we have only fitted the perturbed temperature profiles up to 80 km. We identified two long-period gravity waves having local periods of 6 and 8 hours and corresponding vertical wavelengths of 10 and 15 km, respectively. Note that the background temperature was derived from 4 hours of observation on the night of July 12/13, whereas the derived wave periods are 6 and 8 hours. The estimated temperature perturbations for this night could have been overestimated or underestimated depending on the phases of these waves in the observation period.

Recall the gravity wave parameters that were extracted from the radar data shown in Figure 4. These probably correspond to the local period and vertical wavelength of the 6 hour wave. Closer inspection of Figure 4 provides further support for an 8 hour period wave. Slightly after 1600 LT, at an altitude just over 85 km, faint traces of a second MSE layer can be seen. However, the probability of a strong MSE layer forming at this time is limited by the reduced number of electrons available during the evening. Nevertheless, this presumed weak MSE layer occurs roughly 8 hours after the stronger layer from 0800 to 1400 LT.

All discussions of wave periods are relative to the observer's reference frame. That is, we have not attempted to calculate the intrinsic periods. It is well known that strong horizontal wind velocities can be present near the mesopause, and these winds can Doppler shift the observed frequencies of gravity waves. However, we are not interested in the exact periods of the gravity waves. Rather, we wish to investigate how they might affect the observed temperature field. Since all of our comparisons are made in the observer's frame, the local periods are actually preferred. We note that wind observations collected at Juliusruh (54.63°N, 13.38°E) for July 13 indicate westward and southward winds over the height range of 80–90 km having magnitudes of 26 and 2 m s^{-1}, respectively (P. Hoffmann, private communications, 1996).

Now we are able to model the temperatures in the mesopause region for July 13, 1994. We assume that the wave parameters that were found from the fitting routine represent the dominating perturbing effects to the thermal structure of the atmosphere. Furthermore, we assume that these parameters do not change during the course of the simulation. The modeled temperature T_M is given by

$$T_M(z, t) = T_B(z) + \sum_{n=1}^{N} T_n e^{(z/2H)} \cos(m_n z - \omega_n t + \phi_n) \quad (5)$$

where T_B is the averaged temperature profile for the night of July 12/13 and the gravity wave parameters are those shown in Table 4.

The temperature perturbations predicted by (5) would become artificially large if wave breaking were not considered. Upward propagating gravity waves can break near the mesopause when superadiabatic temperature gradients are produced [*Hodges*, 1967]. The deposited turbulent energy leads, consequently, to a heating of the atmosphere. We have accounted for this in our temperature model by forcing the lapse rate to be less than 10 K km^{-1}.

A time-height contour plot of the temperature for July 13 is shown in Figure 7a. For comparison the vertical beam snr values from the radar observations over the same time and height range are shown in Figure 7b. Although the model used to produce the temperature data is rather simple, several features are evident that support our initial stance. First, a comparison of the radar and simulation data shows that it is reasonable to assume that the dominant MSE layer formed near a trough of the temperature field. We find that the region of the layer associated with the largest snr values corresponds approximately to the lowest temperature values of the trough. Second, the fainter MSE layer found between 1600 and 2000 LT also corresponds to a region of low temperatures. Last, the echo layer occurring slightly below 75 km between 0700 and 1000 LT corresponds to an extended region of reduced temperatures. Likewise, the tail of the dominant MSE layer extends below the height of 75 km.

What temperatures would be needed at a height of 75 km for the ice particles to form? That is, what is the saturation temperature? To answer this question, we again use (2) and pres-

Table 4. Results of the Fitting Routine Using (3) and (4)

Parameter	Definition		Results
Background Temperature			
A	Coefficient		0.119 K km^{-2}
z_{min}	Height of minimum temperature		89.4 km
T_{min}	Minimum temperature		150.8 K
Parameter	**Definition**	**$n = 1$**	**$n = 2$**
Perturbed Temperature			
T_n	Temperature coefficient	0.007 K	0.004 K
ω_n	Local frequency	$2\pi/8$ hours	$2\pi/6$ hours
m_n	Vertical wavenumber	$2\pi/15$ km	$2\pi/10$ km
ϕ_n	Phase angle	0.70	3.1

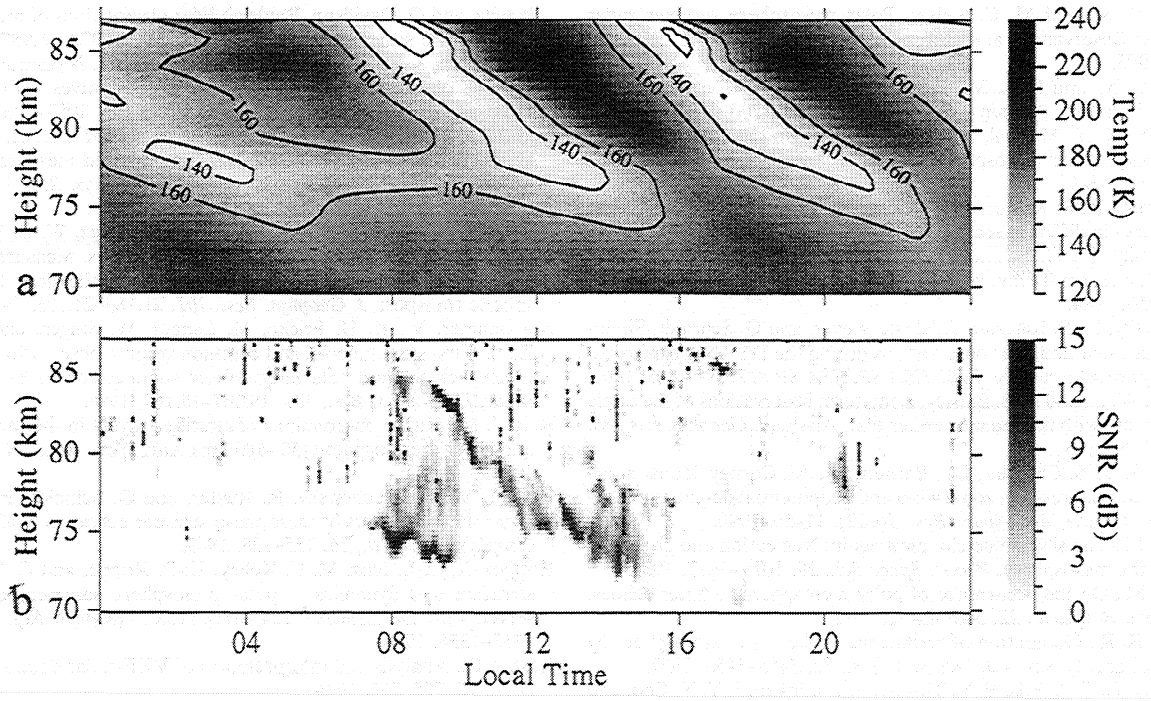

Figure 7. Comparison of the radar observations and the temperature simulations for July 13, 1994: (a) the temperature field simulated using the two-component gravity wave model and (b) the snr for the vertical beam.

sure data from CIRA-86. The value of July at a latitude of 50°N and a height of 75 km is 2.8 Pa. Water mixing ratios have been measured using a ground-based millimeter wave spectrometer [*Nedoluha et al.*, 1995, 1996]. These observations show a seasonal dependence in the water vapor mixing ratio with a peak occurring in the summer months. *Nedoluha et al.* [1996] show at a latitude of 34°N the peak value at 75 km lies near 5 ppmv. Using these values, we find a saturation temperature of 153 K. In the vicinity of the lower layer, there is a cold trough centered at around 78 km with temperatures of approximately 155 K. The trough persists for roughly 6 hours. Considering the temperatures at a height of 75 km for all of July 13, we find that the temperature lies below the 153 K point for 17% of the time. Therefore it is reasonable to assume that the echoes in the 75 km altitude range also represent MSE.

4. Summary

We have presented data collected using the SOUSY VHF radar (51.65°N, 10.49°E) and UV lidar (51.64°N, 10.12°E) in the mesopause region during the summers of 1992 and 1994. These data have been used to investigate the temperature dependence of MSE and to test the assumption that these echoes are related to the presence of subvisible ice particles as proposed by *Inhester et al.* [1994] and *Klostermeyer* [1994, 1996]. On the basis of these observations it has been shown that the MSE layers occur close to heights of minimum temperatures. Similar observations have been reported by *Thomas et al.* [1996]. However, since the lidar measurements presented here and in *Thomas et al.* [1996] are conducted during the night and MSE layers at midlatitudes occur during the day, it is impossible to simultaneously observe a correlation between MSE activity and local temperature.

Nighttime temperature measurements have been extrapolated to daylight hours. The procedure used in our study clearly leads to deviations from the actual temperatures that are difficult to assess. Probably, the largest deviations are caused by the semidiurnal tide. However, since the vertical wavelength of the semidiurnal tide is much larger than those of the observed 6 and 8 hour waves, it should mainly affect the temperature itself rather than the location of the temperature minima.

A closer inspection of Figure 7 indicates that the MSE layers tend to occur mostly below the extrapolated temperature minima. That is, the layers form in a region of steep temperature gradients, in agreement with the results of *Inhester et al.* [1994], *Rüster et al.* [1996], and *Nussbaumer et al.* [1996]. In particular, *Rüster et al.* [1996] discuss high-resolution radar measurements in the summer polar mesosphere that revealed a significant correlation between the snr and the vertical gradient of the potential temperature. The general agreement among the observations may be fortuitous but may, as well, support the suggestion of *Klostermeyer* [1996] that PMSE and MSE are generated at steep gradients of the ice particle concentration which, in turn, are due to temperature gradients close to sufficiently low temperature minima.

Acknowledgments. One of us (PBC) was supported by the Max-Planck-Gessellschaft zur Förderung der Wissenschaft. We extend our gratitude to John Meriwether and Tom VanZandt for their helpful comments.

References

Chanin, M.-L., and A. Hauchecorne, Density and temperature profiles obtained by lidar between 35 and 70 km, *Geophys. Res. Lett.*, *7*, 565–568, 1980.

Chanin, M.-L., and A. Hauchecorne, Lidar observations of gravity and tidal waves in the stratosphere and mesosphere, *J. Geophys. Res.*, *86*, 9715–9721, 1981.

Cho, J. Y. N., and M. C. Kelley, Polar mesosphere summer radar echoes: Observations and current theories, *Rev. Geophys.*, *31*, 243–265, 1993.

Cho, J. Y. N., and R. L. Morley, PMSE dependence on long-period vertical motions, *Geophys. Res. Lett.*, *22*, 1197–1200, 1995.

Cho, J. Y. N., T. M. Hall, and M. C. Kelley, On the role of charged aerosols in polar mesosphere summer echoes, *J. Geophys. Res.*, *97*, 875–886, 1992.

Czechowsky, P., R. Rüster, and G. Schmidt, Variations of mesospheric structures in different seasons, *Geophys. Res. Lett.*, *6*, 459–462, 1979.

Czechowsky, P., G. Schmidt, and R. Rüster, The mobile SOUSY Doppler radar: Technical design and first results, *Radio Sci.*, *19*, 441–450, 1984.

Czechowsky, P., B. Inhester, J. Klostermeyer, and G. Schmidt, Simultaneous radar and lidar observations during the DYANA-campaign, *Eur. Space Agency Spec. Publ. ESA SP, ESA SP-317*, 399–405, 1991.

Ecklund, W. L., and B. B. Balsley, Long-term observations of the arctic mesopause with the radar at Poker Flat, Alaska, *J. Geophys. Res.*, *86*, 7775–7780, 1981.

Fleming, E. J., S. Chandra, J. J. Barnett, and M. Corney, Zonal mean temperature, pressure, zonal wind and geopotential height as a function of latitude, *Adv. Space Res.*, *10*(12), 11–59, 1990.

Gadsen, M., The silver-blue cloudlets again: Nucleation and growth of ice in the mesosphere, *Planet. Space Sci.*, *29*, 1079–1087, 1981.

Hall, C. M., On the occurrence of polar mesosphere summer echoes, *Geophys. Res. Lett.*, *22*, 3469–3472, 1995.

Hodges, R. R., Generation of turbulence in the upper atmosphere by internal gravity waves, *J. Geophys. Res.*, *72*, 3455–3458, 1967.

Hoppe, U. P., T. A. Blix, E. V. Thrane, F.-J. Lübken, J. Y. N. Cho, and W. E. Swartz, Studies of polar mesospheric summer echoes by VHF radar and rocket probes, *Adv. Space Res.*, *14*(9), 139–148, 1994.

Inhester, B., and J. C. Ulwick, Combined rocket and radar observations of anisotropic fluctuations in the mesosphere, *Adv. Space Res.*, *12*(10), 165–168, 1992.

Inhester, B., J. C. Ulwick, J. Y. N. Cho, M. C. Kelley, and G. Schmidt, Consistency of rocket and radar electron density observations: Implications about the anisotropy of mesospheric turbulence, *J. Atmos. Terr. Phys.*, *52*, 855–873, 1990.

Inhester, B., J. Klostermeyer, F.-J. Lübken, and U. von Zahn, Evidence for ice clouds causing polar mesospheric summer echoes, *J. Geophys. Res.*, *99*, 20,937–20,954, 1994.

Jensen, E. J., and G. E. Thomas, Numerical simulations of the effects of gravity waves on noctilucent clouds, *J. Geophys. Res.*, *99*, 3421–3430, 1994.

Kelley, M. C., D. T. Farley, and J. Röttger, The effects of cluster ions on anomalous VHF backscatter from the summer polar mesosphere, *Geophys. Res. Lett.*, *14*, 1031–1034, 1987.

Klostermeyer, J., A two-ion ice particle model of the polar summer mesopause region, *J. Geophys. Res.*, *99*, 5487–5497, 1994.

Klostermeyer, J., On the formation of electron depletions at the summer polar mesopause, *Geophys. Res. Lett.*, *23*, 335–338, 1996.

Lübken, F.-J., and U. von Zahn, Thermal structure of the mesopause region at polar latitudes, *J. Geophys. Res.*, *96*, 20,841–20,857, 1991.

Lübken, F.-J., K.-H. Fricke, M. Langer, P. Hoffmann, W. Singer, B. Inhester, and G. Witt, Simultaneous measurements of noctilucent clouds, polar mesosphere summer echoes, and the temperature near the mesopause, *Eur. Space Agency Spec. Publ. ESA SP, ESA SP (1995)*, pp. 61–66, 1995.

Manson, A. H., J. B. Gregory, and C. E. Meek, Atmospheric waves (~10 min–30 days) in the mesosphere and thermosphere at Saskatoon (52°N, 107°W), October 1978 to September 1979, *Planet. Space Sci.*, *29*, 615–625, 1981a.

Manson, A. H., C. E. Meek, and J. B. Gregory, Winds and waves (10 min–30 days) in the mesosphere and lower thermosphere at Saskatoon (52°N, 107°W, L = 4.3) during the year, October 1979 to July 1980, *J. Geophys. Res.*, *86*, 9615–9625, 1981b.

Meriwether, J. W., P. D. Dao, R. T. McNutt, W. Klemetti, W. Moskowitz, and G. Davidson, Rayleigh lidar observations of mesosphere temperature structure, *J. Geophys. Res.*, *99*, 16,973–16,987, 1994.

Namboothiri, S. P., T. Tsuda, M. Tsutsumi, and T. Nakamura, Simultaneous observations of mesospheric gravity waves with the MU radar and a sodium lidar, *J. Geophys. Res.*, *101*, 4057–1063, 1996.

Nedoluha, G. E., R. M. Bevilacqua, R. M. Gomez, D. L. Thacker, W. B. Waltman, and T. A. Pauls, Ground-based measurements of water vapor in the middle atmosphere, *J. Geophys. Res.*, *100*, 2927–2939, 1995.

Nedoluha, G. E., R. M. Bevilacqua, R.. M. Gomez, W. B. Waltman, B. C. Hicks, D. L. Thacker, and W. A. Matthews, Measurements of water vapor in the middle atmosphere and implications for mesospheric transport, *J. Geophys. Res.*, *101*, 21,183–21,193, 1996.

Nussbaumer, V., K. H. Fricke, M. Langer, W. Singer, and U. von Zahn, First simultaneous and common volume observations of noctilucent clouds and polar mesosphere summer echoes by lidar and radar, *J. Geophys. Res.*, *101*, 19,161–19,167, 1996.

Reid, I. M., Radar observations of stratified layers in the mesosphere and lower thermosphere (50–100 km), *Adv. Space Res.*, *10*(10), 7–19, 1990.

Reid, I. M., P. Czechowsky, R. Rüster, and G. Schmidt, First VHF radar measurements of mesopause summer echoes at midlatitudes, *Geophys. Res. Lett.*, *16*, 135–138, 1989.

Röttger, J., C. L. Hoz, M. C. Kelley, U.-P. Hoppe, and C. Hall, The structure and dynamics of polar mesosphere summer echoes observed with the EISCAT 224 MHz radar, *Geophys. Res. Lett.*, *15*, 1353–1356, 1988.

Rüster, R., Analysis and interpretation of VHF-radar data, *Ann. Geophys.*, *12*, 725–732, 1994.

Rüster, R., Velocity and associated echo power variations in the summer polar mesosphere, *Geophys. Res. Lett.*, *22*, 65–67, 1995a.

Rüster, R., High resolution measurements in the summer polar mesophere, in *STEP Handbook*, edited by B. Edwards, pp. 62–65, Natl. Oceanic and Atmos. Admin., Silver Spring, Md., 1995b.

Rüster, R., P. Czechowsky, P. Hoffmann, and W. Singer, Gravity wave signatures at mesopause heights, *Ann. Geophys.*, *14*, 1186–1191, 1996.

Schmidt, G., R. Rüster, and P. Czechowsky, Complimentary code and digital filtering for detection of weak VHF radar signals from the mesosphere, *IEEE Trans. Geosci. Electron.*, *17*, 154–161, 1979.

Shibata, T., M. Kobuchi, and M. Maeda, Measurements of density and temperature profiles in the middle atmosphere with a XeF lidar, *Appl. Opt.*, *25*, 685–688, 1986.

Sugiyama, T., Y. Muraoka, H. Sogowa, and S. Fukao, Oscillations in polar mesospheric summer echoes and bifurcation of noctilucent cloud formation, *Geophys. Res. Lett.*, *23*, 653–656, 1996.

Thomas, G. E., Mesospheric clouds and the physics of the mesopause region, *Rev. Geophys.*, *29*, 553–575, 1991.

Thomas, L., I. Astin, and T. Prichard, The characteristics of VHF echoes from the summer mesopause region at mid-latitudes, *J. Atmos. Terr. Phys.*, *54*, 969–977, 1992.

Thomas, L., A. K. P. Marsh, D. P. Wareing, I. Astin, and H. Chandra, VHF echoes from midlatitude mesosphere and the thermal structure observed by lidar, *J. Geophys. Res.*, *101*, 12,867–12,877, 1996.

Ulwick, J. C., K. D. Baker, M. C. Kelley, B. B. Balsley, and W. L. Ecklund, Comparison of simultaneous MST radar and electron density probe measurements during STATE, *J. Geophys. Res.*, *93*, 6989–7000, 1988.

P. B. Chilson, Swedish Institute of Space Physics, Box 812, S-981 28 Kiruna, Sweden. (e-mail: phil@irf.se)

P. Czechowsky, J. Klostermeyer, R. Rüster, and G. Schmidt, Max-Planck-Institut für Aeronomie, Postfach 20, D-37189 Katlenburg-Lindau, Germany.

(Received December 12, 1996; revised April 11, 1997;
accepted May 24, 1997.)